PCCP

PAPER

View Article Online
View Journal | View Issue

Cite this: *Phys. Chem. Chem. Phys.*, 2015, **17**, 13575

A molecular dynamics study of $CaCO_3$ nanoparticles in a hydrophobic solvent with a stearate co-surfactant†

Michael S. Bodnarchuk,[a] David M. Heyes,[a] Angela Breakspear,[b] Samir Chahine[b] and Daniele Dini*[a]

Received 23rd January 2015,
Accepted 22nd April 2015

DOI: 10.1039/c5cp00428d

www.rsc.org/pccp

Stearates containing overbased detergent nanoparticles (NPs) are used as acid neutralising additives in automotive and marine engine oils. Molecular dynamics (MD) simulations of the self-assembly of calcium carbonate, calcium stearate as a co-surfactant and stabilising surfactants of such NPs in a model explicit molecular hydrophobic solvent have been carried out using a methodology described first by Bodnarchuk *et al.* [*J. Phys. Chem. C*, 2014, **118**, 21092]. The cores and particles as a whole become more elongated with stearate, and the surfactant molecules are more spaced out in this geometry than in their stearate-free counterparts. The rod dimensions are found to be largely independent of the surfactant type for a given amount of $CaCO_3$. The corresponding particles without stearate were more spherical, the precise shape depending to a greater extent on the chemical architecture of the surfactant molecule. The rod-shaped stearate containing nanoparticles penetrated a model water droplet to a greater depth than the corresponding near-spherical particle, which is possibly facilitated by the dissociation of nanoparticle surfactant molecules onto the surface of the water in this process. These simulations are the first to corroborate the nanoparticle–water penetration mechanism proposed previously by experimental groups investigating the NP acid neutralisation characteristics.

1. Introduction

Calcite, a polymorph of calcium carbonate, is important in Nature (for example in the area of biomineralisation[1]), medicine (as supports for drug delivery[2,3]) and various technological applications and in consumer products.[4] The particle size can affect its physical and chemical properties.[5] Inorganic clusters in solution can adopt a variety of shapes such as flowers,[6] rods,[7] and tetrahedra,[8] which can be controlled using surfactant stabilisers. Calcium carbonate can precipitate in needle shapes,[9] for example. The so-called overbased detergent (OD) chemical is an important class of inorganic–organic hybrid nanoparticle which is added to automotive and marine engine oil to act principally as an acid scavanger.[10–14] The acid neutralising ability is measured using the total base number (TBN), which is the mass in mg of KOH used to neutralise 1 g of the OD detergent.[15] A number of most popular OD surfactants which stabilise the calcium carbonate in oil contain sulphur (*e.g.* sulphonates and SAP, sulphurised alkyl phenates).

Classical theories of micellisation[16] indicate that stearate acting as a co-surfactant could be used to expand the core region isotropically by acting as a 'wedge', allowing it to accommodate more calcium carbonate. This reduces the amount of (stabilising) surfactant required, which is especially important for sulphur-containing surfactants as there is legislation to reduce the amount of sulphur in the OD.[17] The effect of stearate on the state of micellisation and the subsequent acid neutralisation process is still largely unresolved, which is the main focus of this study. Of particular interest is the extent to which the classical picture of micellisation is correct.

There is a history of Molecular Dynamics (MD) computer simulation being applied to model calcium carbonate systems, in more recent times in relation to biomineralisation, for example studies of its growth on ionised organic substrates.[19–26] Molecular dynamics simulations carried out by one of the authors and co-workers of calixarate and phenate-stabilised OD nanoparticles with stearate were reported in 2000.[15] The nanoparticle construction method in that publication started from a largely preformed surfactant-stabilised $CaCO_3$ core to which stearate ions with counter-ions were added. It was concluded that the incorporation of stearate made the nanoparticle more spherical. Our recent simulations of the OD nanoparticle[18] have employed a less biased starting state, in which the chemical components

[a] *Department of Mechanical Engineering, Imperial College London, Exhibition Road, London, SW7, UK. E-mail: m.bodnarchuk@imperial.ac.uk, d.dini@imperial.ac.uk*
[b] *BP Technology Centre, Whitchurch Hill, Pangbourne, RG8 7QR, UK*

† Electronic supplementary information (ESI) available. See DOI: 10.1039/c5cp00428d

and solvent molecules were initially positioned essentially randomly in the simulation cell. The nanoparticle was then free to self-assemble through thermal motion by cooperative arrangement of the species under the influence of the intermolecular force fields. This is the method used in this study. The other novel feature of the present study is the interaction of the nanoparticles with a model water droplet, which is simulated to explore some aspects of the processes leading up to acid neutralisation. Evidence built up from various studies indicates that the $CaCO_3$ core of the OD particle is predominantly amorphous,[12,27–33] making property prediction of calcium carbonate nanoparticles a challenge without adopting computational methods.

2. Simulation details

The OD nanoparticles were stabilised by three different surfactant types, a sulphurised-alkyl phenol (SAP), alkyl-sulphonate and an alkyl-salicylate, as shown in Fig. 1. A co-surfactant, calcium stearate and dispersant molecule were also included in the simulations, whose chemical formulae are also given in Fig. 1.

Two types of self-assembly simulation were performed. In the first (henceforth referred to as the protocol, PI), the calcium and carbonate ions, surfactant and co-surfactant molecules were initially positioned randomly in a model cyclohexane solvent in a periodic cubic MD cell. Cyclohexane is a widely used model hydrophobic solvent in such MD simulations. It has a similar dielectric constant to that of longer alkanes such as decane, and is also typically used to dissolve ODs for their use in engine oils. It is also computationally efficient.

During the simulation these species were observed to self-assemble into an OD nanoparticle. Further equilibration was performed by gradually reducing the ion charges to loosen the structure and then returning the charges to their original values, a procedure described in ref. 18. In ref. 18 it was shown by thermodynamic integration for all the surfactant types used here that the annealing–quenching procedure employed in PI directed the nanoparticle to a lower free energy state.

The second method (henceforth referred to as the protocol, PII) performed the initial OD particle formation without the stearate component. The calcium and stearate ions were then distributed randomly in the simulation cell and allowed to associate with the preformed nanoparticle until a steady state was achieved.

As a further stage in the simulation procedure, the nanoparticles were allowed to interact with a water-droplet consisting of 1000 model water molecules and 23 non-ionic succinimide surfactant molecules,[34] at a temperature of 300 K and a pressure of 1 bar. This type of simulation is the first of its kind.

Succinimide molecules are used as dispersants in engine oil, and it was our purpose to make the medium for the OD particles as close as possible to the real system. It was of interest to explore if they interact with this other type of engine oil additive. It was found that their association with the model overbased particles was not noticeable; they stayed dispersed more or less uniformly in the solvent. This 'negative' result is nevertheless of interest, but because of this result there is no need to comment further on the role of the succinimide molecules here.

The parameters of all the species were obtained using the online Automated Topology Builder (ATB) server,[35,36] and Table 1 gives the number of species included in the different simulations. The quantities of Ca^{2+} and CO_3^{2-} were chosen to give a total base number of approximately 250. This table provides information about the number of various species employed in each of the simulations. The top six rows are for the nanoparticle in a hydrophobic solvent and the bottom three rows are for MD simulations with a water droplet.

Simulations were performed using the Molecular Dynamics (MD) simulation code, GROMACS v4.5.5.[37,38] The particle mesh Ewald method[39] was used to compute the electrostatic terms in the potential, with interactions between atoms within 1.0 nm evaluated every time step and every five steps for atom pairs further apart. Non-bonded van der Waals terms were treated using the Lennard-Jones pair potential with a cut-off of 1.2 nm. Verlet's leapfrog equation of motion integrator was used with a time step of 2 fs. The bond distances and angles of water molecules were constrained using the SETTLE algorithm,[40] and all other bonds were constrained using LINCS.[41] Temperature was regulated using a velocity rescaling thermostat with a coupling time of

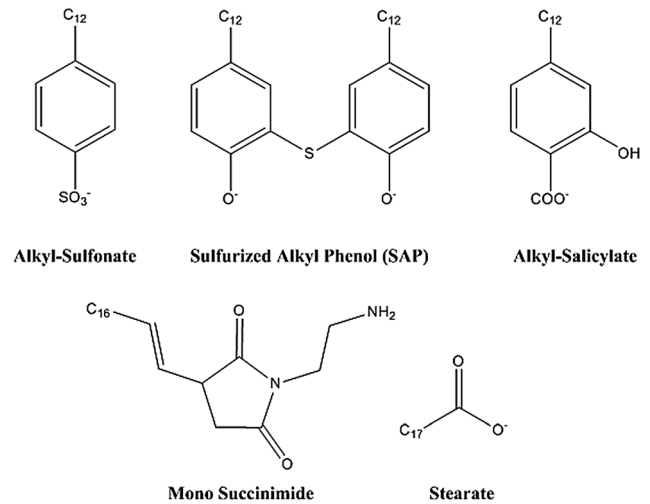

Fig. 1 The three surfactant (alkyl sulfonate, sulfurized alkyl phenate, alkyl salicylate), dispersant (mono succinimide) and co-surfactant (stearate) molecule types used in this study.

Table 1 Summary of the number of each species used for a simulation. Key: S is the surfactant, St is the stearate, Cy is the cyclohexane solvent molecule, and Su is the succinimide dispersant molecule

System	Code	S	St	Cy	Ca^{2+}	CO_3^{2-}	H_2O	Su
SAP	A	6	6	2864	19	10	0	0
Sulphonate	B	12	6	3531	19	10	0	0
Salicylate	C	12	6	3560	19	10	0	0
SAP	D	6	6	3082	29	20	0	0
Sulphonate	E	12	6	3321	29	20	0	0
Salicylate	F	12	6	3510	29	20	0	0
SAP + droplet	G	6	6	5846	29	20	1000	23
Sulphonate + droplet	H	12	6	6355	29	20	1000	23
Salicylate + droplet	I	12	6	5732	29	20	1000	23

0.1 ps,[42–44] and pressure was controlled using the Parrinello–Rahman barostat.[45] Each self-assembly simulation was performed for 40 ns in the NPT ensemble, with structural data collected over the last 5 ns. Simulations containing the nanoparticle formed and a water drop were performed for 20 ns in the NPT ensemble. Structural analysis was performed using the inbuilt GROMACS packages g_sas, g_gyrate and g_dist. The accessible surface area, SA, was found using a probe molecule of diameter, 1.4 Å. The radius of gyration, R_g,[46] is an objective measure of the radius of the particle, which was calculated both for the $CaCO_3$ core and the entire nanoparticle using the respective centre of masses as follows,

$$R_g = \sqrt{\frac{\sum m_i r_i^2}{\sum m_i}}, \quad (1)$$

where r_i is the distance of atom i from the centre of mass of the nanoparticle and m_i its mass.

The shape of the nanoparticle was determined using a literature asphericity order parameter, A_3,[47,48] derived from the moment of inertia tensor which was accumulated during the simulation as follows,

$$A_3 = \frac{\left\langle \sum_{i\neq 1} (\lambda_i - \lambda_j)^2 \right\rangle}{2\left\langle \left(\sum_{i=1}^{3} \lambda_i \right)^2 \right\rangle} \quad (2)$$

where $\langle \cdots \rangle$ denotes a time average and λ_i are the principle moments of inertia of the core. A value of $A_3 = 0$ indicates a sphere and 1, a straight one dimensional rod.

3. Results and discussion

In this section the structural characteristics of the nanoparticles formed in the presence of cyclohexane are discussed. Then the results of MD simulations of the different types of nanoparticles interacting with a water droplet in an explicit hydrophobic solvent are presented and discussed.

3.1. Self-assembly simulations

To assess the influence of stearate on the self-assembly process, the same initial chemical compositions, as previously used for the stearate-free case,[18] were adopted but with an additional six stearate and three Ca^{2+} ions included in the simulation (simulations A to C in Table 1). Two or three nanoparticles were formed during the self-assembly stage, presumably because there was too much surfactant to cover the surface area of the $CaCO_3$ core of a single particle (the total surface area of several nanoparticles is greater than a single one, with the same total amount of calcium carbonate in each case). Doubling the amount of $CaCO_3$ in the mixture to 20 Ca^{2+} ions produced a single nanoparticle (simulations D to F in Table 1).

The structural characteristics of the SAP, sulphonate and salicylate-based nanoparticles formed in the presence of stearate are summarised in Table 2.

Table 2 Key structural characteristics of the three types of nanoparticles constructed using protocols, PI and PII. SA is the accessible surface area. The radii of gyration, R_g, for the core and total nanoparticle are also given. The standard deviation of the radius of gyration is reported in parentheses. A_3 is the asphericity parameter defined in eqn (2) for the whole particle

Surfactant	Method	Core SA/nm^2	R_g-core/nm	R_g-total/nm	A_3
SAP	PI	12.73 (0.20)	0.89 (0.01)	1.45 (0.02)	0.14
Sulphonate	PI	12.54 (0.28)	0.93 (0.01)	1.48 (0.01)	0.15
Salicylate	PI	12.31 (0.37)	0.91 (0.05)	1.52 (0.02)	0.13
SAP	PII	12.08 (0.21)	0.62 (0.01)	1.10 (0.01)	0.04
Sulphonate	PII	11.23 (0.22)	0.59 (0.02)	1.16 (0.02)	0.03
Salicylate	PII	11.58 (0.23)	0.68 (0.02)	1.14 (0.02)	0.06

Table 2 shows that the surface area, radius of gyration and asphericity parameter of the nanoparticles are smaller when the stearate is added after the main core had formed (*i.e.*, using PII) compared with the PI strategy. Also within the set of surfactant types there is a statistically significant variation in these quantities in the PII case. This is similar to what was previously found by simulations performed without stearate,[18] which also produced a sulphonate nanoparticle in which the core was more compact (*i.e.*, with a smaller radius of gyration) than that formed from the other two surfactant classes. In ref. 18 it was shown by thermodynamic integration for all the surfactant types used here that the annealing–quenching procedure employed in PI directed the nanoparticle to a lower free energy state compared to previous self-assembly strategies. The same behaviour was observed in this study. The SAP, sulphonate and salicylate nanoparticles formed during PI were found to be stabilised by −2750, −3000 and −2920 kJ mol^{-1}, respectively, upon annealing. In comparison, the addition of stearate post core formation was found to stabilise the particles by only approximately −1000 kJ mol^{-1}. The PI procedure produced nanoparticles with a lower free energy than those formed by PII which did not allow the stearate molecules to fully relax into the nanoparticle during an annealing process. Nanoparticles formed using PI therefore have a lower thermodynamic free energy and more closely resemble those made experimentally.

The nanoparticles are more rod-shaped when produced using PI, as is evident by comparing the A_3 values for the PI and PII sets. The PII-type nanoparticles are significantly more spherical, suggesting that the addition of stearate after the initial core had formed does not allow sufficient time for rearrangement to a rod-like shape to occur during a typical simulation time (*i.e.*, the activation free energy being too high compared with k_BT).

The PI structural descriptors of Table 2 are statistically indistinguishable for the three surfactant types. The negative charge surrounding the stearate head-group is more localised than for the sulphonate surfactant, and is therefore likely to dominate the structure of that type of nanoparticle.

Completed simulation snapshots of the sulphonate-based stearate containing nanoparticle at the end of the 40 ns PI and PII procedures are shown in Fig. 2, which confirm what can be inferred from Table 2 that the PI procedure produces a more elongated core and rod shaped particle.

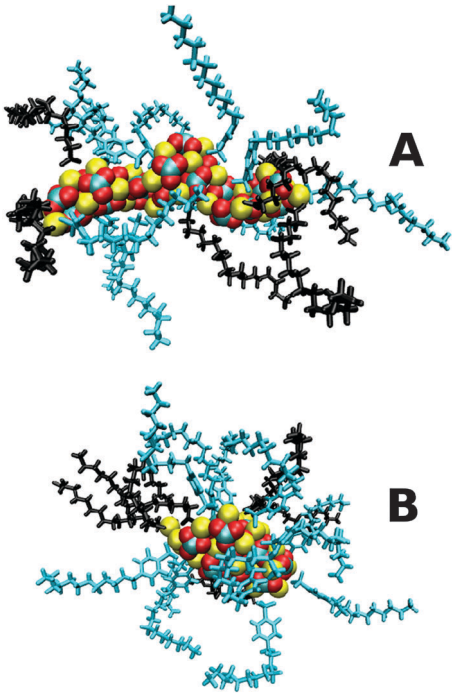

Fig. 2 Simulation snapshots of the sulphonate-based nanoparticle. (A) Stearate added during the self-assembly process, PI. (B) Stearate added post self-assembly, PII. Calcium ions are shown in yellow, and cyan and red indicate the carbon and oxygen atoms of the carbonate ions, respectively. The sulphonate surfactant is shown in cyan, with the stearate co-surfactant shown in black.

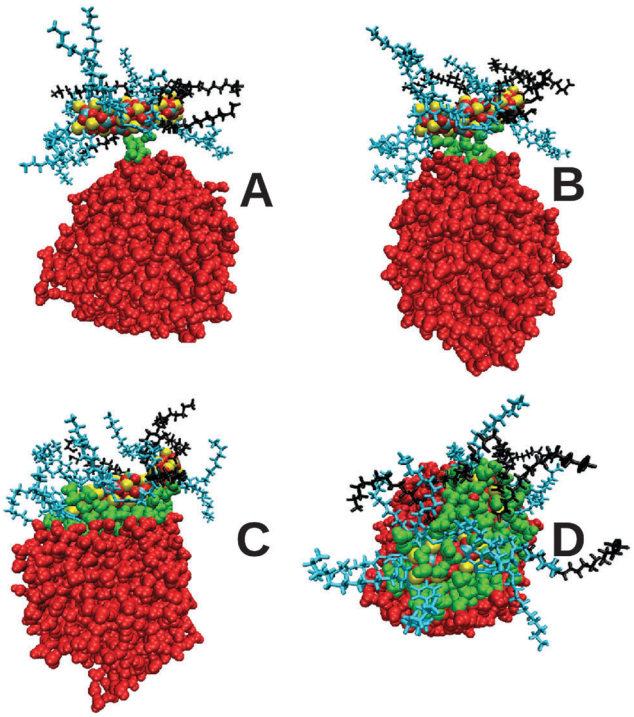

Fig. 3 MD snapshots during a 20 ns simulation of a SAP/stearate nanoparticle and a representative water droplet, showing the successive stages of (A) initial bridge formation, (B) bridge development, (C) water coating of the nanoparticle, and (D) full nanoparticle adsorption into the water drop. Water molecules within 7 Å of the nanoparticle are shown as green spheres, with the rest represented by red spheres. Calcium ions are shown in yellow. The cyan and red spheres represent the carbon and oxygen atoms, respectively, of the carbonate ions. The SAP surfactants are shown in cyan, with the stearate co-surfactant shown in black.

The results are consistent with experimental evidence,[7,49] and theory,[50] that rod-shaped surfactants tend to form rod-shaped micelles. The stearate co-surfactant has a significantly smaller head-group than the three main surfactants used to stabilise the nanoparticle, promoting the formation of a rod-shaped particle. The surfactant molecules are more spaced out along the rod (frame (a)) than for the more spherically shaped particle (frame (b)), hence the insensitivity of the core surface area and radii of gyration to the surfactant type in the PI class of nanoparticles. It may be concluded that the nanoparticle produced in this study using PI is closer to the optimal free energy structure compared to the original work performed some 15 years ago when computer resources and software capability were more limited.[15] The experimental systems are therefore more likely to resemble those shown in Fig. 2A than Fig. 2B.

3.2. Interaction with water

The primary role of overbased detergents is to neutralise acidic byproducts of combustion inside automotive and marine engines. The acids (mainly nitric and sulphuric acid) are formed from combustion gases dissolved in the water droplets present in the lubricant. There is some evidence that the overbased detergents attach onto water droplets *via* a three stage process.[51,52] First, the overbased nanoparticle diffuses by thermal motion close to a water droplet. Then a water bridge is formed between the two particles. Finally, water molecules increasingly coat the OD nanoparticle, forming a strong interface between the two and which allows more ready neutralisation of any acid in the water droplet (the acid is not included in these simulations). This proposed mechanism is predominantly based upon reaction rate experiments and microcapilliary visualisations, and to the knowledge of the authors no simulations have been carried out to confirm or refute this mechanism.

Fig. 3 and 4 for the SAP-stearate and sulphonate-stearate particles formed using PI (simulations G and H in Table 1), respectively, demonstrate that this proposed mechanism is supported by the MD simulations (the behaviour of the salicylate nanoparticle, simulation I, is shown in the ESI†). A short-lived bridge is formed within 500 ps, before the water molecules begin to coat the core. In both cases, the OD nanoparticle fully attaches itself to the water droplet. The majority of the core had penetrated into the droplet approximately 2 ns after the initial bridge formation. Note that in Fig. 3 and 4 the water molecules which are within 7 Å of the core are shown in green.

All three nanoparticles demonstrate some degree of surfactant dissociation from the $CaCO_3$ core which is possibly driven by the larger number of potentially favourable calcium ion–water interactions, which outweigh the interactions between the surfactant molecules and the core. The surfactant-dissociation facilitates increased core penetratation into the water droplet since the presence of a surfactant acts as a hydrophobic steric barrier

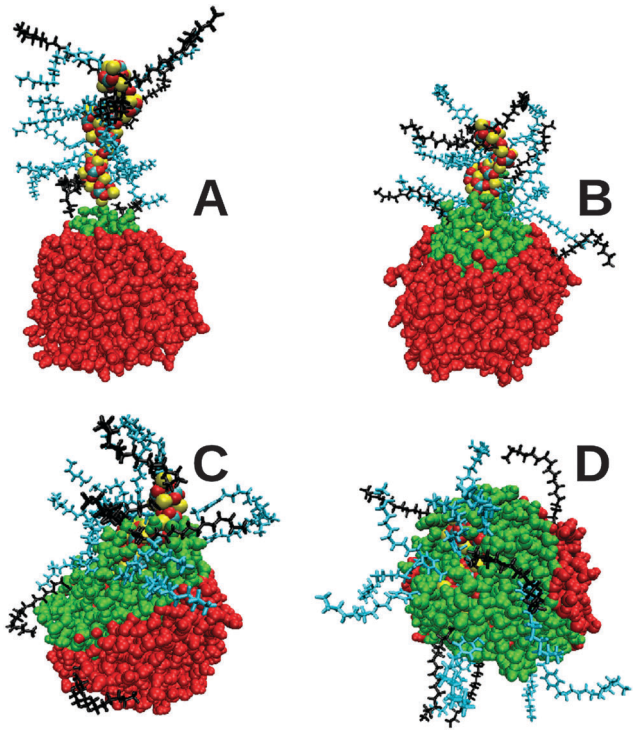

Fig. 4 As for Fig. 3 except the behaviour of the sulphonate/stearate nanoparticle is shown.

between the core and water. In all cases the accessible hydrophobic surface area of the core upon penetration is zero, indicating close to total coverage of the core by the water droplet. Fig. 6A shows that, for the sulphonate case, most of the core is surrounded by water molecules in the final stages, with a number of surfactant molecules distributed around the droplet surface. Fu and co-workers have shown that increased neutralisation rates are found for overbased particles containing surfactants which can dissociate from the $CaCO_3$ core,[53,54] and these simulations give support to this view in that increased penetration of the core into an acidic droplet will accompany partial dissociation of the surfactant molecules from the nanoparticle.

Successful core-droplet docking was observed in approximately three out of four simulations, independent of the surfactant type. As a prelude to the absorption the initial angle of approach between the core and the droplet varied. An equal number of side-on (Fig. 3A) and head-on (Fig. 4A) approaches was observed, suggesting that there is no favoured orientation for attachment to occur.[55] The two approaches took between 1 and 5 ns to yield fully immersed cores, further suggesting that there is no significant dependence of outcome on the angle of approach.

The same simulations were performed for the spherical stearate-containing particles formed using PII. Fig. 5 shows how the distance between the centre of mass for the PI and PII nanoparticles and the water droplet changes upon initial contact between the two species.

The spherical nanoparticle formed using PII does not penetrate as much into the water droplet compared to PI. Treating the

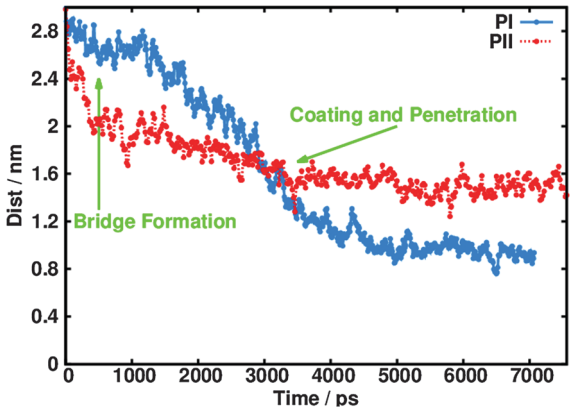

Fig. 5 Variation in the distance between the centre of mass of the nanoparticle and the water droplet as a function of time after initial contact is made.

entire NP as a single entity or an effective 'molecule', the total interaction energy between the NP and the water was -9600 kJ mol^{-1} for the sulphonate PI particle and -6400 kJ mol^{-1} for the PII particle, highlighting that more favourable interactions are made with the more penetrative rod-shaped particle. The time for immersion into the droplet is broadly similar for the two procedures after initial bridge formation (PI: 4 ns, PII: 3 ns).

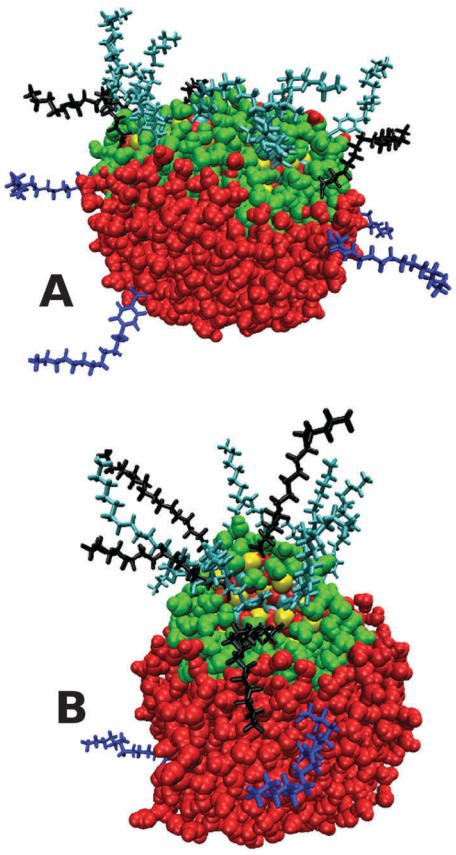

Fig. 6 MD snapshots at the end of a 20 ns simulation of a sulphonate/stearate nanoparticle (PI = A, PII = B) and a representative water droplet, showing the dissociated surfactant molecules (in blue) from the core. The same colour scheme as Fig. 3 is used for the molecules.

Adsorption of the PII $CaCO_3$ core into the droplet occurred in only about one in five of the simulations, with approximately half the number of surfactants dissociated from the core compared to PI. Fig. 6B shows the fully immersed core alongside the dissociated sulphonate surfactants, and demonstrates the reduced penetration into the middle of the droplet.

The reduced frequency of successful dockings using the PII particles suggests that shape is both an important factor in the adsorption of overbased detergents and also the degree of penetration into the water droplet.

Such factors could have implications for the rate of reaction for such detergents. It is reasonable to assume that species which penetrate deeper and more frequently into water droplets will have an increased rate of reaction due to a larger reactive interface with the acid.[53,54] This work has shown that molecular simulations could have potential in helping us to predict surfactants which form more water-accessible nanoparticles, which will be more reactive.

4. Conclusions

This work builds on previous molecular simulations by some of us which concluded that the shape and size of nanoparticles can be controlled by the choice of stabilising surfactant type.[18] The MD simulations carried out here suggest that stearate acting as a co-surfactant in the synthesis of overbased detergents causes a major change in particle shape, and potentially reactivity as an acid neutralisation agent. This co-surfactant induces a normally near-spherical nanoparticle to adopt a rod-like shape, whose dimensions are less dependent on the chemical formula of the surfactant stabiliser than is the case for nanoparticles formed without the stearate additional component. Although these are not typical micellar systems, in having a solid core with specific surfactant binding criteria, the classical literature description and the explanation of the influence of a cosurfactant as causing a uniform 'swelling' of a micelle does not appear to be applicable to this class of nanoparticles. The transformation into a more rod shaped structure could affect its diffusional behaviour in the oil of an automotive or marine engine and even perhaps the rate of reaction with acid in water droplets found therein. When exposed to a model water droplet, incorporated in the computer model as a new feature, the stearate co-surfactants were found to dissociate from the core, thereby allowing the nanoparticle to absorb deeper into the droplet where the core ions on the surface can interact energetically favourably with the water molecules. Previous simulations[18] only investigated the effects of trace water on the carbonate core, and not with a similarly sized water droplet to the nanoparticle. These simulations are therefore the first of their kind and are a significant step towards the molecular modelling of the overbased detergent function in a realistic chemical environment.

The results corroborate the experimentally-derived hypothesis which relates the strength of nanoparticle–water association to surfactant dissociation onto the surface of the water droplet during this process. The reduced water penetration of a more spherical particle (formed here by adding stearate late in the self-assembly process) suggests that the shape of the nanoparticle is an important factor in governing the mechanism and kinetics of the assocation process of the overbased particle with bulk water, as a precursor to the process of acid neutralisation. It is reasonable to assume that nanoparticles which adsorb deeper into a water droplet will exhibit faster reaction times because of the greater exposure of the core to any acid in the water.

Such studies may ultimately help us to identify promising chemical compositions for overbased detergents which have reduced sulphur content and favourable neutralisation kinetics tailored to the demands of specfic types of engine operation.

Acknowledgements

M.S.B. thanks BP for the award of a Research Fellowship.

References

1 J. H. Harding and D. M. Duffy, *J. Mater. Chem.*, 2005, **16**, 1105–1112.
2 Y. Ueno, H. Futagawa, Y. Takagi, A. Ueno and Y. Mizushima, *J. Controlled Release*, 2005, **103**, 93–98.
3 D. Shan, M. Zhu, H. Xue and S. Cosnier, *Biosens. Bioelectron.*, 2007, **22**, 1612–1617.
4 U. Aschauer, D. Spagnoli, P. Bowen and S. C. Parker, *J. Colloid Interface Sci.*, 2010, **346**, 226–231.
5 C. Y. Tai and C.-K. Chen, *Chem. Eng. Sci.*, 2008, **63**, 3632–3642.
6 W. L. Noorduin, A. Grinthal, L. Mahadevan and J. Aizenberg, *Science*, 2013, **340**, 832–837.
7 J. B. F. N. Engberts and J. Kevelam, *Curr. Opin. Colloid Interface Sci.*, 1996, **1**, 779–789.
8 M.-P. Pileni, *Nat. Mater.*, 2003, **2**, 145–150.
9 F. Rauscher, P. Veit and K. Sundmacher, *Colloids. Surf., A*, 2005, **254**, 183–191.
10 C. L. Lee, P. J. Dowding, A. R. Doyle, K. M. Bakker, S. S. Lam, S. E. Rogers and A. F. Routh, *Langmuir*, 2013, **13**, 14763–14771.
11 J. A. Griffiths, R. Bolton, D. M. Heyes, J. H. Clint and S. E. Taylor, *J. Chem. Soc., Faraday Trans.*, 1995, **91**, 687–696.
12 J. A. Griffiths and D. M. Heyes, *Langmuir*, 1996, **12**, 2418–2424.
13 C. A. Bearchell, D. M. Heyes, D. J. Moreton and S. E. Taylor, *Phys. Chem. Chem. Phys.*, 2001, **3**, 4774–4783.
14 C. A. Bearchell, J. A. Edgar, D. M. Heyes and S. E. Taylor, *J. Colloid Interface Sci.*, 1999, **210**, 231–240.
15 C. Bearchell, T. Danks, D. M. Heyes, D. J. Moreton and S. E. Taylor, *Phys. Chem. Chem. Phys.*, 2000, **2**, 5197–5207.
16 J. N. Israelachvilli, *Intermolecular and Surface Forces*, Academic Press, London and New York, 2nd edn, 1991.
17 EMSA, *The 0.1 sulphur in fuel requirement as from 1 January 2015 in SECAs*, Lisbon, 2010.
18 M. S. Bodnarchuk, D. M. Heyes, D. Dini, S. Chahine and S. Edwards, *J. Phys. Chem. C*, 2014, **118**, 21092–21103.
19 D. M. Duffy and J. H. Harding, *J. Mater. Chem.*, 2002, **12**, 3419–3425.

20 D. M. Duffy and J. H. Harding, *Langmuir*, 2004, **20**, 7637–7642.
21 D. M. Duffy and J. H. Harding, *Surf. Sci.*, 2005, **595**, 151–156.
22 C. L. Freeman, J. H. Harding and D. M. Duffy, *Langmuir*, 2008, **24**, 9607–9615.
23 D. Quigley, P. M. Rodger, C. L. Freeman, J. H. Harding and D. M. Duffy, *J. Chem. Phys.*, 2008, **131**, 094703.
24 J. P. Allen, A. Marmier and S. C. Parker, *J. Phys. Chem. C*, 2012, **116**, 13240–13251.
25 J. P. Allen, S. C. Parker and M. S. D. Read, *Geochim. Cosmochim. Acta*, 2009, **73**, A29.
26 J. P. Allen, S. C. Parker and D. W. Price, *Geochim. Cosmochim. Acta*, 2008, **72**, A16.
27 V. Bakunin, A. Suslov, G. Kuzmina, O. Parenago and A. Topchiev, *J. Nanopart. Res.*, 2004, **6**, 273–284.
28 L. K. Hudson, J. Eastoe and P. J. Dowding, *Adv. Colloid Interface Sci.*, 2006, **123–126**, 425–431.
29 B. Niemann, F. Rauscher, D. Adityawarman, K. Voigt and A. Sundmacher, *Chem. Eng. Process.*, 2006, **45**, 917–935.
30 D. Quigley and P. M. Rodger, *J. Chem. Phys.*, 2008, **128**, 221101.
31 F. Nudelman, E. Sonmezler, P. H. H. Bomans, G. de With and N. A. J. M. Sommerdijk, *Nanoscale*, 2010, **2**, 2436–2439.
32 D. Liu, M. Zhang, G. Zhao and X. Wang, *Tribol. Lett.*, 2011, **45**, 265–273.
33 F. Gilberti, G. A. Tribello and M. Parrinello, *J. Chem. Theory Comput.*, 2013, **9**, 2526–2530.
34 A. Tomlinson, T. N. Danks, D. M. Heyes, S. E. Taylor and D. J. Moreton, *Langmuir*, 1997, **13**, 5881–5893.
35 A. K. Malde, L. Zuo, M. Breeze, M. Stroet, D. Poger, P. C. Nair, C. Oostenbrink and A. E. Mark, *J. Chem. Theory Comput.*, 2011, **7**, 4026–4037.
36 S. Canzar, M. El-Kebir, R. Pool, K. Elbassioni, A. E. Mark, D. P. Geerke, L. Stougie and G. W. Klau, *J. Comput. Biol.*, 2013, **20**, 188–198.
37 D. Van Der Spoel, E. Lindahl, B. Hess, G. Groenhof, A. E. Mark and H. J. C. Berendsen, *J. Comput. Chem.*, 2005, **26**, 1701–1718.
38 S. Pronk, S. Páll, R. Schulz, P. Larsson, P. Bjelkmar, R. Apostolov, M. R. Shirts, J. C. Smith, P. M. Kasson, D. van der Spoel, B. Hess and E. Lindahl, *Bioinformatics*, 2013, **29**, 845–854.
39 U. Essmann, L. Perera, M. L. Berkowitz, T. Darden, H. Lee and L. G. Pedersen, *J. Chem. Phys.*, 1995, **103**, 8577–8593.
40 S. Migamoto and P. A. Kollman, *J. Comput. Chem.*, 1992, **13**, 952–962.
41 B. Hess, H. Bekker, H. J. C. Berendsen and J. G. E. M. Fraaije, *J. Comput. Chem.*, 1997, **18**, 1463–1472.
42 G. Bussi, D. Donadio and M. Parrinello, *J. Chem. Phys.*, 2007, **126**, 014101.
43 L. V. Woodcock, *Chem. Phys. Lett.*, 1971, **10**, 257–261.
44 S. Nosé, *Prog. Theor. Phys. Suppl.*, 1991, **103**, 1–46.
45 M. Parrinello and A. Rahman, *J. Appl. Phys.*, 1981, **52**, 7182–7190.
46 N. Cooper, A. Tedder, D. M. Heyes and J. R. Melrose, *J. Phys.: Condens. Matter*, 1989, **1**, 6217–6230.
47 J. Rudnick and G. Gaspari, *J. Phys. A: Math. Gen.*, 1986, **19**, L191–L193.
48 J. Rudnick and G. Gaspari, *Science*, 1987, **237**, 384–389.
49 J. J. H. Nusselder and J. B. F. N. Engberts, *J. Org. Chem.*, 1991, **56**, 5522–5527.
50 J. N. Israelachvili, D. J. Mitchell and B. J. Ninham, *J. Chem. Soc., Faraday Trans.*, 1976, **2**, 1525–1568.
51 R. C. Wu, C. B. Campbell and K. D. Papadopoulos, *Ind. Eng. Chem. Res.*, 2000, **39**, 3926–3931.
52 R. C. Wu, K. D. Papadopoulos and C. B. Campbell, *AIChE J.*, 2000, **46**, 1471–1477.
53 J. Fu, Y. Lu, C. B. Campbell and K. D. Papadopoulos, *Ind. Eng. Chem. Res.*, 2006, **45**, 5619–5627.
54 J. Fu, Y. Lu, C. B. Campbell and K. D. Papadopoulos, *Tribol. Lett.*, 2006, **22**, 221–225.
55 R. Aveyard, B. D. Beake and J. H. Clint, *J. Chem. Soc., Faraday Trans.*, 1996, **92**, 4271–4277.